Stratospheric correlation between nitric acid and ozone

P. J. Popp,[1,2,3] T. P. Marcy,[1,2] R. S. Gao,[1] L. A. Watts,[1,2] D. W. Fahey,[1] E. C. Richard,[4] S. J. Oltmans,[5] M. L. Santee,[6] N. J. Livesey,[6] L. Froidevaux,[6] B. Sen,[6] G. C. Toon,[6] K. A. Walker,[7] C. D. Boone,[8] and P. F. Bernath[8,9]

Received 29 July 2008; revised 24 November 2008; accepted 12 December 2008; published 12 February 2009.

[1] An extensive data set of nitric acid (HNO_3) and ozone (O_3) measurements has been collected in the lower and middle stratosphere with in situ instruments onboard the NASA WB-57F aircraft and remote sounding instruments that include the JPL MkIV Interferometer, the Aura Microwave Limb Sounder, and the Atmospheric Chemistry Experiment Fourier Transform Spectrometer. The measurements utilized in this study span a broad latitudinal range between the deep tropics and northern high latitudes. The data are used to establish the robustness of the HNO_3-O_3 correlation in the stratosphere and the latitudinal dependence in the correlation. Good agreement is found among the HNO_3-O_3 correlations observed with the various instruments. Comparing HNO_3-O_3 correlations relaxes the coincidence criteria necessary when making direct comparisons of HNO_3 measurements and allows meaningful comparisons between data sets that are not closely matched in time or space. The utility of this correlation is further demonstrated by establishing vertical profiles of proxy HNO_3 mixing ratios using the observed correlation and widely available ozonesonde data. These profiles expand the range of data available for validating remote measurements of HNO_3. The HNO_3-O_3 correlation is also demonstrated as a diagnostic for identifying locally enhanced HNO_3 in the upper troposphere. In situ measurements of HNO_3 near the tropical tropopause during the Aura validation campaigns are consistent with ACE-FTS observations, with both revealing extremely low mixing ratios (<125 ppt) and a HNO_3 minimum in this region.

Citation: Popp, P. J., et al. (2009), Stratospheric correlation between nitric acid and ozone, *J. Geophys. Res.*, *114*, D03305, doi:10.1029/2008JD010875.

1. Introduction

[2] Nitric acid (HNO_3) is a principal component of total reactive nitrogen (NO_y) in the stratosphere. NO_y also includes the other oxides of nitrogen, such as NO_x (the sum of NO and NO_2). Since the catalytic destruction of ozone (O_3) by NO_x is one of the dominant O_3 loss mechanisms in the stratosphere, HNO_3 is indirectly involved in controlling stratospheric ozone concentrations [*Farman et al.*, 1985; *Brasseur and Solomon*, 2005]. HNO_3 also plays a key role in the formation of polar stratospheric clouds (PSCs) in polar winters. Surface reactions on PSCs cause the formation of reactive chlorine species in the wintertime polar stratospheres, and thus facilitate ozone loss processes in these regions [*Solomon*, 1999; *Gao et al.*, 2001]. Outside of the polar regions, O_3 can generally be considered a long-lived tracer in the lower stratosphere and has been used as a diagnostic for transport and dynamic processes [*Bregman et al.*, 2000; *Hegglin and Shepherd*, 2007; *Marcy et al.*, 2007]. HNO_3 and O_3 exhibit a strong positive correlation in the lower stratosphere [*Neuman et al.*, 2001]. Correlations between HNO_3 and O_3 have previously been used to characterize air masses in the Arctic and midlatitude lower stratospheres [*Bregman et al.*, 1995; *Schneider et al.*, 1999; *Neuman et al.*, 2001], validate HNO_3 profiles [*Irie et al.*, 2006] and describe tracer relationships in the tropical tropopause layer (TTL) [*Marcy et al.*, 2007].

[3] We report here an extensive data set of HNO_3 and O_3 measurements collected in the lower and middle stratosphere. The data were collected using both in situ instruments onboard the NASA WB-57F aircraft and a suite of balloon- and satellite-borne remote sounding instruments. The measurements are used here to establish the robustness of the HNO_3-O_3 correlation in the stratosphere, characterize the

[1]Chemical Sciences Division, Earth System Research Laboratory, National Oceanic and Atmospheric Administration, Boulder, Colorado, USA.
[2]Cooperative Institute for Research In Environmental Sciences, University of Colorado, Boulder, Colorado, USA.
[3]Now at Leeds School of Business, University of Colorado, Boulder, Colorado, USA.
[4]Laboratory for Atmospheric and Space Physics, University of Colorado, Boulder, Colorado, USA.
[5]Global Monitoring Division, Earth System Research Laboratory, National Oceanic and Atmospheric Administration, Boulder, Colorado, USA.
[6]Jet Propulsion Laboratory, California Institute of Technology, Pasadena, California, USA.
[7]Department of Physics, University of Toronto, Toronto, Ontario, Canada.
[8]Department of Chemistry, University of Waterloo, Waterloo, Ontario, Canada.
[9]Department of Chemistry, University of York, York, UK.

0148-0227/09/2008JD010875

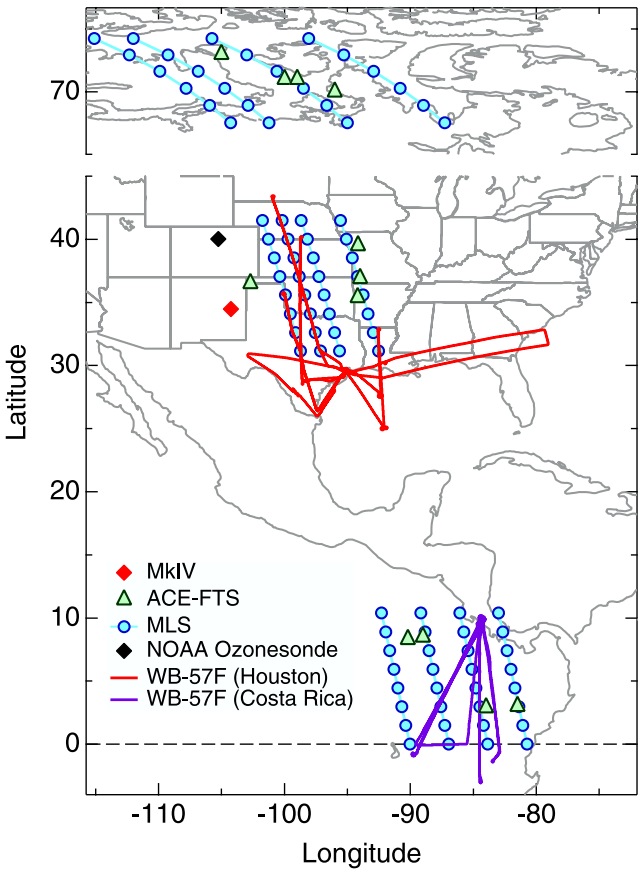

Figure 1. Measurement locations for data sets utilized in this study. MkIV is part of the Balloon Observations of the Stratosphere gondola launched from Fort Sumner, New Mexico. Symbols representing the ACE-FTS and MLS measurements show the location of individual profiles. Ozonesondes were launched from the NOAA/ESRL station in Boulder, Colorado. Flight tracks of the NASA WB-57F aircraft show the location of in situ data collected as part of the AVE-Houston and Costa Rica measurement campaigns.

latitudinal variability in the correlation, and illustrate the utility of the correlation for validating remote sounding instrumentation.

2. Observations

[4] Measurements of HNO_3 and O_3 mixing ratios were made in situ with instruments onboard the NASA WB-57F high-altitude research aircraft. HNO_3 was measured using the NOAA Chemical Ionization Mass Spectrometer (CIMS) [*Neuman et al.*, 2000; *Marcy et al.*, 2005], with a reported accuracy of ±25% and a 1-σ precision of 40 ppt or better. O_3 was measured with an overall uncertainty of ±5% by the NOAA Ozone Photometer [*Proffitt et al.*, 1983]. Measurements were made in the tropical lower stratosphere during four flights conducted as part of the NASA Pre-Aura Validation Experiment (Pre-AVE) in January and February 2004 and Costa Rica Aura Validation Experiment (CR-AVE) in February 2006 (Figure 1). We believe these data represent the first in situ measurements of HNO_3 in the tropical lower stratosphere. The flights originated and terminated at Juan Santamaria International Airport near San Jose, Costa Rica (10°N, 84°W). In situ measurements were also made in the midlatitude lower stratosphere over the continental United States during six flights as part of the Aura Validation Experiment-Houston (AVE-Houston) campaign in June 2005 (Figure 1). These flights originated and terminated at Ellington Field in Houston, Texas (30°N, 95°W).

[5] This study also utilizes HNO_3 and O_3 measurements from three different remote sounding instruments; the Aura Microwave Limb Sounder (MLS), the JPL MkIV Interferometer (MkIV), and the Atmospheric Chemistry Experiment Fourier Transform Spectrometer (ACE-FTS). Of the data available from each of these instruments, we have chosen to utilize limited subsets that are coordinated temporally and/or geographically with the in situ measurements and each other as much as possible. The MLS instrument, onboard the Earth Observing System Aura satellite, quantifies HNO_3 and O_3 by measuring thermal emission from the limb of Earth's atmosphere [*Waters et al.*, 2006]. The MLS version 2.2 data has an overall uncertainty of ±2 ppb or better in the HNO_3 retrievals and ±10% in the O_3 retrievals throughout the vertical range of the data described here (147–22 hPa) [*Santee et al.*, 2007; *Froidevaux et al.*, 2008]. Vertical and horizontal resolutions of the MLS measurements are 3–4 km and ~400 km, respectively. We utilize MLS data from four Aura overpasses in each of 3 distinct latitudinal regions; 0°–10°N over the tropical eastern Pacific Ocean, 31°N–41°N over the continental United States, and 68°N–74°N over the Canadian Arctic (Figure 1). The tropical MLS data were chosen to match the location and season of the WB-57F Costa Rica flights and ACE-FTS occultations, but were collected between 29 January and 4 February 2005 because MLS data are not available during this time period in 2004. The midlatitude MLS data were collected during the WB-57F AVE-Houston campaign, on 13, 15, 17 and 22 June 2005. Two of the WB-57F flights (on 13 and 22 June) were coordinated to align with the Aura ground tracks near the time of the satellite overpass for validation purposes [*Santee et al.*, 2007]. The Arctic MLS data were collected on the same days as ACE-FTS occultations in this region (15 September and 29 October 2005, and 30 October and 20 November 2006).

[6] The MkIV Interferometer is a balloon-borne solar-occultation Fourier transform spectrometer that measures infrared spectra at sunrise or sunset with a spectral resolution of 0.01 cm^{-1} [*Toon*, 1991]. Systematic uncertainties for MkIV retrievals of HNO_3 and O_3 in the stratosphere are 12% and 6%, respectively. The vertical resolution of the MkIV measurements is 2–3 km. We utilize MkIV profiles of HNO_3 and O_3 observed during three balloon flights from Fort Sumner, New Mexico (34°N, 104°W), on 19 September 2003, 23 September 2004, and 20 September 2005 (Figure 1).

[7] The ACE-FTS instrument, also a solar-occultation Fourier transform spectrometer, is onboard the Canadian Space Agency's SCISAT-1 satellite [*Bernath et al.*, 2005; *Boone et al.*, 2005]. ACE-FTS measures high-resolution (0.02 cm^{-1}) infrared spectra with global coverage from 85°S to 85°N. The ACE-FTS statistical fitting errors are ~5% or better for stratospheric mixing ratios of HNO_3 and O_3 in the version 2.2 (and version 2.2 "O_3 update") data

retrievals [*Wolff et al.*, 2008; *Dupuy et al.*, 2008]. Vertical and horizontal resolutions of the ACE-FTS measurements are 3–4 km and ~500 km, respectively. We utilize 4 ACE-FTS profiles from three latitudinal regions similar to those chosen for the MLS data; 3°N–8°N over the tropical eastern Pacific Ocean (7 February and 6 April 2004, 25 April 2006, and 22 February 2007), 35°N–40°N over the continental United States (29 and 30 July 2004, and 5 June and 31 July 2005), and 70°N–73°N over the Canadian Arctic (15 September and 29 October 2005, and 30 October and 20 November 2006) (Figure 1). The tropical profiles were chosen to match as closely as possible the location and season of the WB-57F Costa Rica flights and MLS overpasses, and the midlatitude profiles were chosen to match the location and season of the WB-57F AVE-Houston flights and MLS overpasses. Some of these profiles were not sampled in the same year as the WB-57F or MLS data owing to the relatively sparse sampling of the ACE-FTS occultations in the tropics and midlatitudes.

[8] Vertical profiles of O_3 mixing ratio were measured at the NOAA Earth Systems Research Laboratory (NOAA/ESRL) ozonesonde station in Boulder, CO (40°N, 105°W) (Figure 1). The NOAA/ESRL network uses electrochemical-concentration-cell ozonesondes with an accuracy of ±10% [*Newchurch et al.*, 2003]. We utilize the O_3 profiles from sonde flights on June 20 and 24 of 2005 during the WB-57F AVE-Houston campaign.

3. Results and Discussion

[9] In situ measurements onboard the NASA WB-57F during the AVE-Houston campaign reveal a robust and compact correlation between HNO_3 and O_3 in the midlatitude lower stratosphere (Figure 2a). A least squares regression analysis of the decile averages (unfilled black symbols) in Figure 2a indicates a linear relationship between HNO_3 and O_3 over the range of the data shown. Deciles, defined as representing an equal number of data points, have the advantage over binned averages in that they reveal the density of points in Figure 2a. The regression algorithm is only applied to data with O_3 greater than 150 ppb to prevent enhanced values of HNO_3 in the troposphere from compromising the fit (see large values of HNO_3 at ~100 ppb O_3 in Figure 2a). These enhanced values of HNO_3 in the troposphere will be discussed later. There is no observable latitudinal dependence in the HNO_3-O_3 correlation greater than the natural variability over the limited latitudinal range of the data shown (24°N–43°N). The observed dependence over a larger latitude range is discussed in section 3.2. The precisions of the in situ measurements near 2 ppb HNO_3 and 750 ppb O_3 are displayed with the error bar symbol in the bottom right corner of Figure 2a. The precision of each tracer measurement is derived as the standard deviation of the 10-s averages during flight segments with near-constant average values. These values are substantially less than the observed scatter in the 10-s data (Figure 2a), indicating that the latter results primarily from the small-scale geophysical variability of HNO_3 and O_3 in the stratosphere.

[10] A comparison of in situ measurements onboard the WB-57F and remote measurements from the MkIV, ACE-FTS and MLS instruments in the midlatitude lower stratosphere is shown in Figure 2b. The remote sounding data do

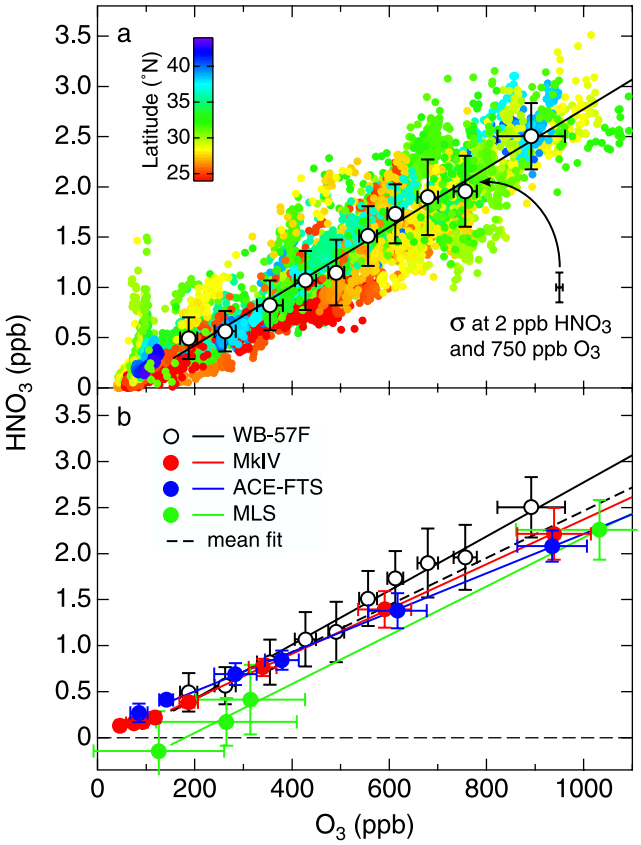

Figure 2. (a) HNO_3-O_3 correlation observed in the midlatitude lower stratosphere. Colored data points are 10-s averages (4900 in total) of in situ measurements onboard the NASA WB-57F. Data are colored as a function of measurement latitude (see Figure 1). The symbol in the bottom right corner shows the precision of the 10-s HNO_3 and O_3 measurements at 2 ppb HNO_3 and 750 ppb O_3. The black open symbols represent averages of the 10-s data divided into deciles (10 equally sized bins), with error bars representing the standard deviation of the decile averages. Only data at ozone values greater than 150 ppb are included in the deciles. The linear fit to the in situ data is calculated using the decile averages. (b) HNO_3-O_3 correlations observed with in situ and remote sounding instruments. Black open symbols are the decile averages of the in situ data shown in Figure 2a. The remote sounding data represent averages of data as reported for their respective retrieval levels. MkIV data represent average values from three balloon flights. ACE-FTS data represent average values from four occultations. MLS data represent average values combined from eight profiles on each of four Aura overpasses. Error bars for each represent the standard deviation of the average values. Linear fits are shown as calculated with the MkIV, ACE-FTS, and MLS data averages (equally weighted) excluding data at O_3 mixing ratios less than 150 ppb. A combined linear fit of the averages (or deciles) from all four data sets (equally weighted) is also shown in Figure 2b excluding O_3 mixing ratios less than 150 ppb.

not represent decile averages, but rather averages of data as reported at their respective retrieval levels (see Figure 2 caption). All of these data were collected at latitudes between 24°N and 43°N (Figure 1), and during the months of June, July or September to coincide temporally and geographically with the WB-57F data set. Thus, seasonal effects are not expected to contribute significantly to the differences in the HNO_3-O_3 correlations shown here. All of the data averages above 150 ppb O_3 in Figure 2b, with the exception of the MLS values at 265 ppb and 315 ppb O_3, lie within ±15% of a linear fit calculated using all 4 data sets combined with equal weighting. The low values of HNO_3 observed in the MLS correlation (at O_3 mixing ratios less than 400 ppb) result from the known low bias in the MLS HNO_3 data in the upper troposphere and lowermost stratosphere [*Santee et al.*, 2007]. The equation for the least squares linear regression is given by

$$HNO_3 = (0.00256 \pm 0.000154) \cdot (O_3) - (0.0922 \pm 0.0886)$$

with HNO_3 and O_3 expressed in ppb for the range 150 ppb $< O_3 <$ 1100 ppb. The coefficient of determination (R^2) for the linear fit to the combined data set is 0.93, indicating that the HNO_3-O_3 correlation is robust in the midlatitude lower stratosphere and comparable between data sets that are measured with a variety of in situ and remote techniques.

[11] The use of in situ data for the validation of remote sounding instruments can be influenced by two issues that make meaningful comparisons between the data sets challenging. First, in situ measurements from aircraft platforms typically have horizontal resolutions of a few kilometers (~1.8 km for the 10-s data in Figure 2a) and are reported at a specific altitude, whereas the remote measurements considered here have horizontal resolutions of hundreds of kilometers and vertical resolutions up to several kilometers. Thus, the small-scale geophysical variability of HNO_3 observed with in situ measurements (as seen in Figure 2a) cannot be detected by remote sounding instruments that report average conditions over considerably larger sampling volumes. Second, most remote measurements are ideally validated using data sets that are approximately coincident in time and space. Coincidence criteria vary depending on the measurements being compared [e.g., *Walker et al.*, 2005; *Santee et al.*, 2007; *Considine et al.*, 2008] but most comparisons involve data obtained within a few hours and 500 km of each other [*Hegglin et al.*, 2008]. Given these requirements, sufficient data are not always available to provide statistically significant comparisons. Both of these issues can largely be overcome, however, if a robust relationship exists between the species A of interest and another species B, like that shown in Figure 2, and if measurements of both species are simultaneously available from the same platform. The best cases occur when species A and B are long-lived tracers. Tracer correlations provide a so-called "instantaneous climatology" that reduces the influence of small-scale geophysical variability observed in in situ data sets and has allowed a meaningful comparison between data sets with measurements having vastly different sampling volumes [e.g., *Hegglin et al.*, 2008; *Nightingale et al.*, 1996; *Khosrawi et al.*, 2004]. For example, *Murphy et al.* [1993] have demonstrated that the variability of the NO_y to O_3 ratio (HNO_3 is a primary component of NO_y) is significantly lower than the variability of either species observed individually in the lower stratosphere. Furthermore, the instantaneous climatology provided by robust tracer correlations relaxes the coincidence criteria necessary when making direct comparisons of HNO_3 measurements and allows statistically meaningful comparisons between a variety of data sets that are not closely matched in time or space (Figure 2b).

[12] When using HNO_3-O_3 correlations as a tool for validating HNO_3 measurements, there is an implicit assumption that the uncertainty in the O_3 measurement is less than the uncertainty in the HNO_3 measurement from the same platform. This assumption is valid in many cases because O_3 is usually given a higher measurement priority than HNO_3, and there are usually more options available for validating O_3 measurements. The relative uncertainty for O_3 is less than the relative uncertainty for HNO_3 in all of the data sets utilized here with the exception of the ACE-FTS measurements. (The ACE-FTS data set has a reported error of ~5% in both the HNO_3 and O_3 measurements.) Nonetheless, when a comparison between data sets using HNO_3-O_3 correlations reveals systematic differences, the possibility that the differences result from the O_3 measurements rather than the HNO_3 measurements must also be considered. Identifying the origin(s) of differences then requires more than one diagnostic. Ideally, the HNO_3-O_3 correlations are but one diagnostic in a comprehensive validation of remote HNO_3 and O_3 measurements.

[13] There is no direct chemical connection between HNO_3 and O_3 to explain the strong positive correlation between the two species [*Murphy et al.*, 1993]. Both are produced by photochemical processes in the middle stratosphere, predominately in the tropics where ultraviolet radiation is most intense, and both have long photochemical lifetimes in the lower stratosphere [*Brasseur and Solomon*, 2005]. The correlation results because both HNO_3 and O_3 are long-lived species with common stratospheric source regions, and are therefore subject to the same transport and mixing processes once they are formed [*Murphy et al.*, 1993]. These common features produce similar vertical gradients for the two species throughout the lower and middle stratosphere. The correlation is not linear throughout this region because the region of net maximum O_3 production extends higher in the middle stratosphere than that for HNO_3 and total reactive nitrogen is destroyed in the upper stratosphere (Figure 3) [*Fahey et al.*, 1990]. Remote measurements from the MkIV, ACE-FTS and MLS instruments at altitudes up to 30 km indicate HNO_3 mixing ratios reach a maximum at $(5-6)\cdot 10^3$ ppb of O_3 (~25 km) and then decrease at larger O_3 mixing ratios (higher altitudes). The strong agreement between the HNO_3-O_3 correlations in the MkIV, ACE-FTS and MLS data sets at midlatitudes is evident in Figure 3. The coefficients for the second-order polynomial fits to the correlations are shown in Table 1. The correlation in the MLS data suggests that the MLS HNO_3 retrievals are systematically low by ~0.5–1 ppb between 25 km and 30 km altitude, consistent with conclusions reported by *Santee et al.* [2007]. The data in Figure 3 represent measurements obtained over a 3-year period (2003 to 2005), further illustrating the utility of the HNO_3-O_3 correlation as a validation tool when comparing noncoincident measurements.

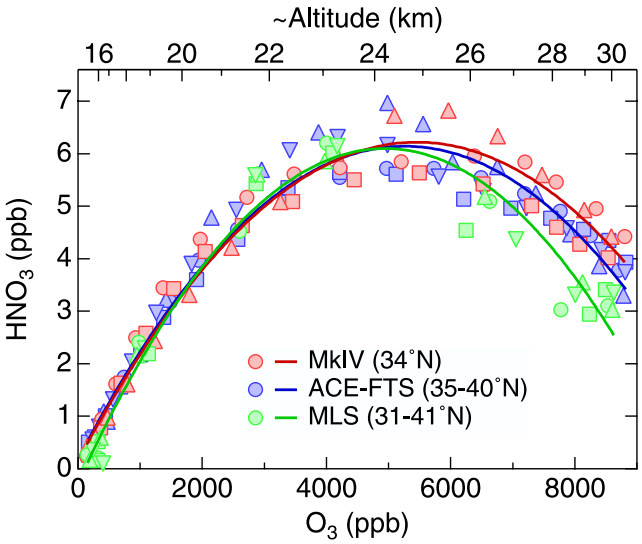

Figure 3. HNO_3-O_3 correlations observed by the MkIV, ACE-FTS and MLS instruments in the midlatitude stratosphere (see Figure 1). Different symbols shapes represent individual occultations (three for MkIV, four for ACE-FTS) or different satellite overpasses (MLS, with eight profiles averaged during each of four overpasses). Lines represent second-order polynomial fits to the combined data set of each instrument. The coefficients for the polynomial fits are shown in Table 1.

3.1. Calculating Proxy HNO_3 Profiles

[14] In situ measurements of HNO_3 onboard the NASA WB-57F have proven to be useful for the validation of MLS HNO_3 retrievals in the lower stratosphere [*Santee et al.*, 2007]. Despite the higher natural variability displayed in the in situ measurements, coincident HNO_3 measurements from the WB-57F and MLS on 22 June 2005 generally show fair-to-good agreement when the two data sets are compared without smoothing for a single day as shown in Figure 4. A limitation of such comparisons is that the maximum flight altitude of the WB-57F allows comparison only as high as the 68 hPa MLS retrieval level (Figure 4). Using the well-characterized stratospheric correlation between HNO_3 and O_3, however, we can calculate a proxy profile of HNO_3, designated H HNO_3*, from in situ ozonesonde data. Vertical profiles of O_3 mixing ratio from ozonesondes are more widely available and typically extend to higher altitudes than aircraft data sets. O_3 profiles were available from the NOAA/ESRL Boulder ozonesonde station on 20 and 24 June 2005, 2 days before and after the WB-57F and MLS measurements shown in Figure 4. A HNO_3* profile was calculated by applying the polynomial equation for the midlatitude ACE-FTS HNO_3-O_3 correlation (Figure 3 and Table 1) to the average of the two ozonesonde profiles (Figure 4). The HNO_3* profile agrees within expected uncertainties with the WB-57F and MLS data throughout most of the vertical range shown in Figure 4. The average MLS value at 22 hPa is approximately 1 ppb lower than HNO_3*, consistent with known biases in the MLS data set in this region [*Santee et al.*, 2007]. The variability in HNO_3* results from the uncertainties associated with the specific HNO_3-O_3 correlation relation and O_3 measurements being used. If an averaged and smoothed O_3 profile is used to estimate HNO_3*, then the variability in the real atmospheric HNO_3 abundances will be underrepresented by HNO_3*.

[15] The use of HNO_3-O_3 correlations to calculate HNO_3* from in situ ozonesonde profiles expands the range of data available for validating remote measurements of HNO_3. Unlike a direct comparison of HNO_3-O_3 correlations for the purpose of validation, as described above, this method does not require a simultaneous O_3 measurement from the platform being validated. We also note that the utility of HNO_3* profiles is not limited to the validation of remote sounding instrumentation, since they can be used whenever high-resolution vertical profiles of HNO_3 are required. This method offers the advantage that daily variations in the vertical structure of the stratosphere, particularly near the tropopause, will be evident in the ozonesonde data and thus accounted for in the calculation of HNO_3*.

3.2. Latitudinal Dependence in the HNO_3-O_3 Correlation

[16] The near-global coverage of satellite-borne remote sounding instruments makes them ideally suited to studying latitudinal variations in the HNO_3-O_3 correlation. Measurements in the Northern Hemisphere tropical, midlatitude and polar stratosphere by the ACE-FTS and MLS instruments reveal a strong latitudinal dependence in the correlation and good agreement between the two instruments (Figure 5). The coefficients for the second-order polynomial fits to the correlations are given in Table 1. The latitudinal dependence illustrated in Figure 5 is best explained as an evolution from initial conditions represented by the tropical correlation. When air moves upward through the tropical stratosphere via the large-scale ascent that is part of the Brewer-Dobson circulation [*Brewer*, 1949], O_3 is produced more efficiently than HNO_3 resulting in the relatively low HNO_3/O_3 and NO_y/O_3 ratios observed in this region [*Fahey et al.*, 1996]. As air moves poleward and ages, HNO_3/O_3 ratios increase

Table 1. Coefficients for the Second-Order Polynomial Fits to the HNO_3-O_3 Correlations Shown in Figures 3 and 5[a]

Instrument and Location	a	b	c	Range (ppb)
ACE-FTS (70°N–73°N)	−0.42279	0.0048101	-5.7629×10^{-7}	$150 < O_3 < 6600$
ACE-FTS (35°N–40°N)	0.17878	0.0022653	-2.1521×10^{-7}	$150 < O_3 < 8800$
ACE-FTS (3°N–8°N)	0.11311	0.00074318	-4.4215×10^{-8}	$150 < O_3 < 1 \times 10^5$
MkIV (34°N)	0.15818	0.0022216	$-2.0400 \cdot 10^{-7}$	$150 < O_3 < 8800$
MLS (68°N–74°N)	−1.1311	0.0045093	$-5.2908 \cdot 10^{-7}$	$150 < O_3 < 6600$
MLS (31°N–41°N)	−0.27047	0.0025794	$-2.6100 \cdot 10^{-7}$	$150 < O_3 < 8800$
MLS (0°–10°N)	1.1949	9.9836×10^{-5}	-1.1119×10^{-9}	$150 < O_3 < 1 \times 10^5$

[a]The polynomial equation takes the form $HNO_3 = a + b(O_3) + c(O_3)^2$, with HNO_3 and O_3 both in units of parts per billion.

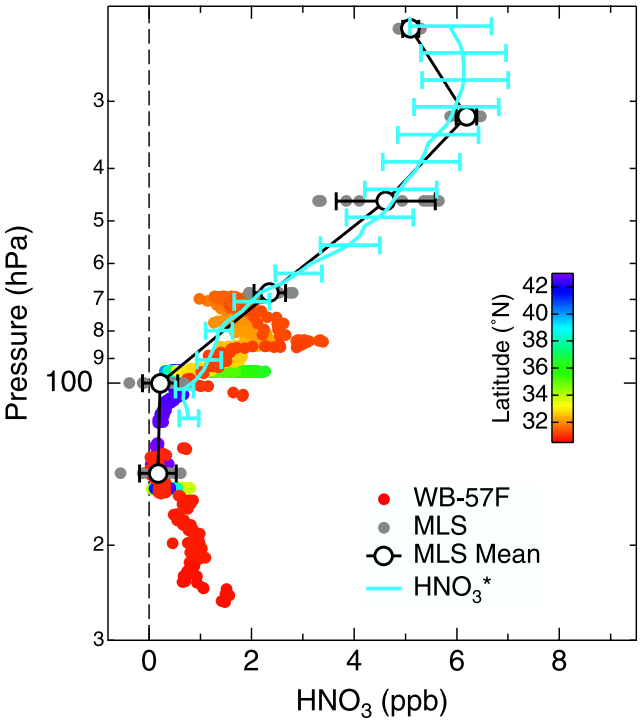

Figure 4. Vertical profiles of HNO_3 mixing ratio from the WB-57F and MLS on 22 June 2005 during the AVE-Houston validation campaign. WB-57F data are colored as a function of latitude. MLS data represents eight vertical profiles at latitudes of 31°N–41°N as reported at standard MLS retrieval levels. HNO_3* was calculated using the average of two ozonesonde profiles at 40°N on 20 and 24 June 2005 and the polynomial fit for the midlatitude ACE-FTS HNO_3-O_3 correlation shown in Table 1. The HNO_3* error bars represent the combined uncertainties of the ozonesonde profiles and polynomial fit to the mid-latitude HNO_3-O_3 correlation.

owing to the greater net production of HNO_3. The only significant loss of HNO_3 (or, more generally, loss of NO_y) meanwhile, occurs at altitudes greater than 40 km owing to the photolytic destruction of NO and the subsequent repartitioning of the NO_y reservoir [*Fahey et al.*, 1990].

[17] *Murphy et al.* [1993] have described a similar latitudinal dependence on linear NO_y-O_3 correlations observed at altitudes up to 21 km in the lower stratosphere. NO_y/O_3 ratios do not increase smoothly between the tropics and high latitudes, but are instead separated by two regions with very strong gradients in the ratio; in the subtropics between 12° and 22° latitude, and at the edge of the polar regions at ~65°. The strong gradients are due to weak horizontal mixing in these regions [*Murphy et al.*, 1993; *Fahey et al.*, 1996]. In regions between these two sharp gradients, namely in the tropics, midlatitudes and polar regions (as depicted in Figure 5), the NO_y-O_3 correlation is much less variable. We expect the HNO_3/O_3 ratio to exhibit a similar behavior in the lower stratosphere with only minor variability in the tropics, midlatitudes and polar regions, and sharp gradients in the transition regions because HNO_3 is generally a large fraction of NO_y in the lower stratosphere [*Neuman et al.*, 2001]. *Hegglin and Shepherd* [2007] have observed that the correlation between O_3 and nitrous oxide (N_2O) is compact in the lower stratosphere but relatively less compact in the middle stratosphere, revealing a fan-like structure in the correlation when data over a broad and continuous latitudinal range are included. We note that the HNO_3-O_3 correlations in Figure 5 are expected to display a similar change in compactness if data from a broad and continuous latitudinal range were to be included.

[18] *Murphy et al.* [1993] reported little seasonal variation in the NO_y-O_3 correlation in the tropics and midlatitudes, and a more significant seasonal variation displayed in the correlation measured at high latitudes primarily associated with processes in the wintertime polar vortex. For this

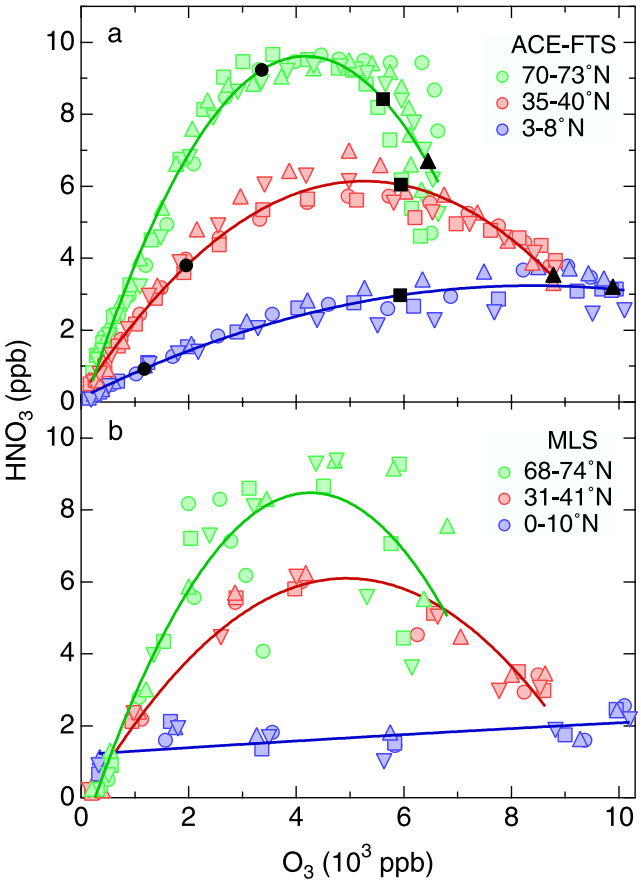

Figure 5. (a) HNO_3-O_3 correlations observed by the ACE-FTS instrument in the Northern Hemisphere tropics (3°N–8°N), midlatitudes (35°N–40°N), and polar regions (70°N–73°N). The correlations were established using data from four occultations in each region, represented by the different symbol shapes. The coefficients for the second-order polynomial fits to each correlation are shown in Table 1. Approximate measurement altitudes are represented by black circles, squares, and triangles at 20, 25, and 30 km, respectively. (b) HNO_3-O_3 correlations observed by the MLS instrument in the Northern Hemisphere tropics (0°–10°N), midlatitudes (31°N–41°N), and polar regions (68°N–74°N). The correlations were established using data from four overpasses in each region, represented by the different symbol shapes. The coefficients for the second-order polynomial fits to each correlation are shown in Table 1.

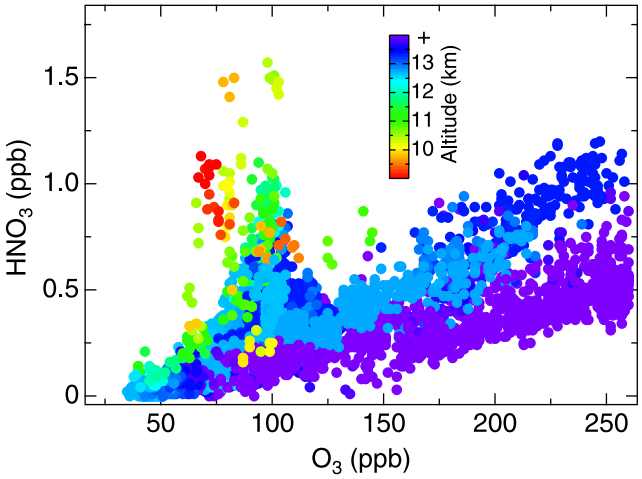

Figure 6. HNO_3-O_3 correlation observed in the midlatitude upper troposphere and lower stratosphere with in situ measurements onboard the NASA WB-57F. Data are displayed as 1-s averages and are colored as a function of measurement altitude.

reason, the polar correlations shown in Figure 5 were chosen from data collected in the late summer or early fall in order to minimize any potential effects from denitrification [*Santee et al.*, 2000; *Fahey et al.*, 1990] and chemical ozone loss [*Solomon*, 1999] that might perturb the HNO_3-O_3 correlation.

3.3. HNO_3-O_3 Correlations in the Midlatitude Upper Troposphere

[19] The HNO_3-O_3 correlation in the upper troposphere can be linear and compact owing to the mixing of air masses between the stratosphere and troposphere. Similar linear and compact HCl-O_3 correlations in the upper troposphere were used previously to derive the fraction of stratospheric air in the midlatitude upper troposphere [*Marcy et al.*, 2004]. The HNO_3-O_3 correlation in the upper troposphere, however, is typically less compact than the stratospheric correlation [*Murphy et al.*, 1993; *Neuman et al.*, 2001]. The source of this variability lies in the fact that O_3 is long-lived and generally well mixed throughout the upper troposphere while HNO_3 is subject to local production and removal. For example, redistribution through uptake and sedimentation by cirrus cloud particles is considered an important term in the upper tropospheric budget of HNO_3 [*Lawrence and Crutzen*, 1998; *Popp et al.*, 2004, 2007; *Krämer et al.*, 2008]. Nonetheless, the correlation between HNO_3 and O_3 can serve as a useful diagnostic for locally enhanced values of HNO_3 in the upper troposphere. Enhanced HNO_3 mixing ratios as large as 1.5 ppb were observed over the midlatitude upper troposphere during four of six AVE-Houston WB-57F flights (Figure 6, at 50–125 ppb O_3). We argue that this enhanced HNO_3 is produced locally in the upper troposphere by the oxidation of lightning-produced NO_x [*Murphy et al.*, 1993; *Martin et al.*, 2007, and references therein]. The upper tropospheric lifetime of NO_x against conversion to HNO_3 is ~5 days [*Jaeglé et al.*, 1998]. These enhancements cannot be stratospheric in origin because the stratospheric HNO_3-O_3 correlation (at O_3 > 150 ppb in Figure 6) would be preserved upon transport and dilution in the upper troposphere. It is also unlikely that the enhanced HNO_3 mixing ratios are due to anthropogenic or natural emissions at Earth's surface, since most NO_x is converted to HNO_3 in the boundary layer. This HNO_3 is unlikely to reach the upper troposphere in convection since the rainout lifetime of a highly soluble species like HNO_3 near the surface is typically less than 3 days [*Giorgi and Chameides*, 1986] and HNO_3 is efficiently removed during upward transport. Previous NO_x measurements in the outflow of summertime thunderstorms over the continental United States revealed lightning-produced NO_x mixing ratios as large as 4 ppb at 9–12 km altitude, consistent with the altitudes of enhanced HNO_3 shown in Figure 6 [*Ridley et al.*, 1996, *Martin et al.*, 2007].

3.4. HNO_3 and O_3 in the Tropical Upper Troposphere and Lower Stratosphere

[20] HNO_3 and O_3 measurements have unique features in the tropical upper troposphere and lower stratosphere. In situ measurements of HNO_3 in the deep tropics (3°S–10°N) onboard the WB-57F indicate a minimum in HNO_3 at altitudes of 14–17 km in the TTL (Figure 7a). Observed HNO_3 mixing ratios were typically 125 ppt or less throughout this region. Remote measurements by the ACE-FTS instrument show slightly larger HNO_3 mixing ratios that are nonetheless consistent with the upper range of the in situ measurements (Figure 7). While the HNO_3 minimum is not apparent in the ACE-FTS measurements reported here because the minimum measurement altitude is 15.5 km, a previous study utilizing a larger subset of the ACE-FTS measurements does indicate a similar HNO_3 minimum in the tropical upper troposphere [*Folkins et al.*, 2006]. Convective transport models have been used to simulate the HNO_3 minimum observed in the tropics [*Folkins et al.*, 2006], although the minimum predicted by the models occurs at 13–14 km altitude, which is 3–4 km lower than found in the in situ data set presented here. The models attribute the HNO_3 minimum to the convective outflow of air that is depleted in HNO_3 [*Folkins et al.*, 2006], . Simulations with a wet-convection plume model indicate that HNO_3 scavenging is highly efficient in deep convective updrafts, and that as little as 3% of HNO_3 entrained in the cloud column will be detrained at anvil height [*Mari et al.*, 2000]. We note that condensed-phase HNO_3 has been observed in subvisible cirrus clouds at altitudes of 16–18 km in the tropics [*Popp et al.*, 2007]. Under appropriate conditions, the vertical redistribution of HNO_3 by uptake and sedimentation in cirrus ice particles could provide an additional sink of HNO_3 in the TTL. The convective plume model described by *Folkins et al.* [2006] does not account for the redistribution of HNO_3 in ice particles, and would tend to underpredict the height of the HNO_3 minimum if this process is a significant factor in the HNO_3 budget in the TTL. Finally, although the increase in HNO_3 above 18 km (Figure 7a) is due to photochemical production and transport from the middle stratosphere, HNO_3 mixing ratios are lower in the tropics than at higher latitudes (at similar altitudes) in part because air entering the tropical lower stratosphere through the TTL is depleted in HNO_3.

[21] The elevated HNO_3 mixing ratios at altitudes less than 14 km in Figure 7 suggest a source of HNO_3 in the tropical troposphere, which is most likely the oxidation of

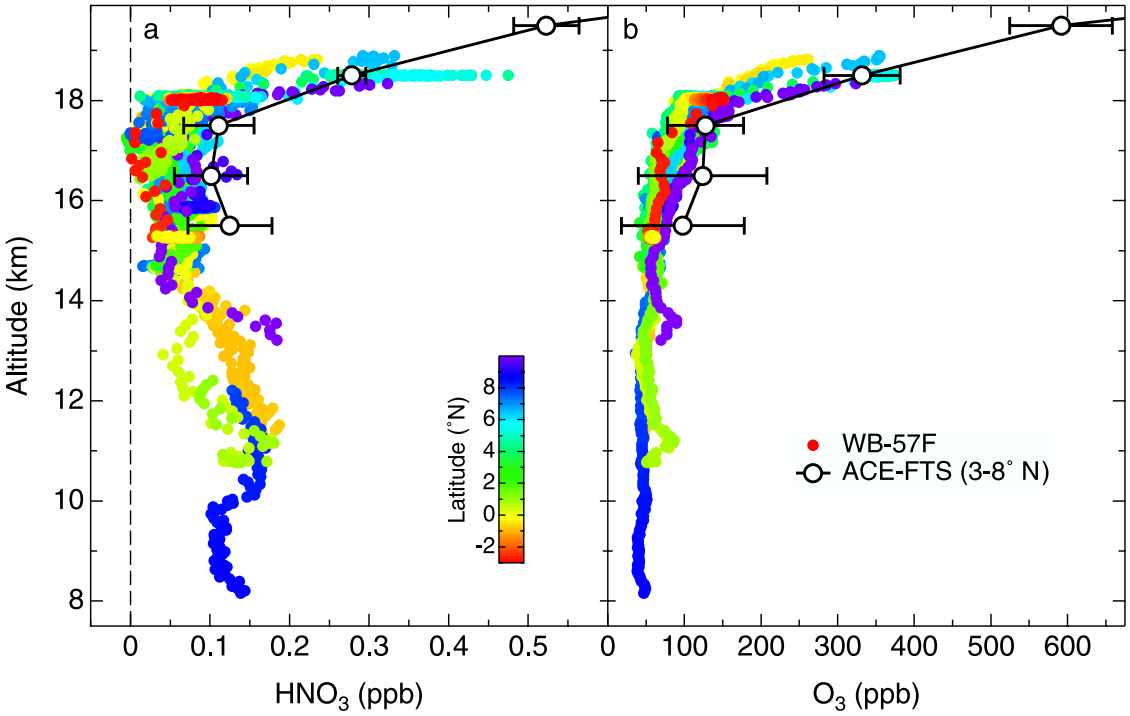

Figure 7. (a) Vertical profiles of HNO_3 in the tropics. In situ measurements onboard the NASA WB-57F are colored as a function of measurement latitude and are displayed as 10-s averages. ACE-FTS symbols represent the average HNO_3 mixing ratio from four occultations, and error bars represent the standard deviation of the average values. (b) Vertical profiles of O_3 in the tropics. Details same as Figure 7a.

lightning-produced NO_x. *Martin et al.* [2007] have reported that nearly 80% of the HNO_3 between 8.5 km and 12.5 km altitude in the tropics can be explained by lightning production. Since the data shown in Figure 7 represent maritime measurements, and lightning occurs more frequently over the continents, we caution that the tropospheric HNO_3 data in Figure 7 might be biased low compared to continental data and thus should not be interpreted as a tropical climatology.

[22] In situ measurements of O_3 in the tropics show a largely monotonic increase in O_3 between the upper troposphere and lower stratosphere, with no evidence of an O_3 minimum in the TTL (Figure 7b) since O_3 is not efficiently scavenged in convective updrafts. Remote measurements by the ACE-FTS instrument indicate O_3 mixing ratios that are largely consistent with the in situ measurements but show a slight high bias with respect to the in situ observations. A high bias of ACE-FTS O_3 in the extratropical upper troposphere was noted by *Hegglin et al.* [2008]. Like HNO_3, the increase in O_3 above 18 km altitude is due to photochemical production and transport from the middle stratosphere. Unlike HNO_3, O_3 is not produced in significant amounts by lightning in the upper troposphere and O_3 is not removed in convective updrafts. Approximately half of the O_3 in the TTL is photochemically produced in situ, with the remainder contributed either by the tropospheric background or mixing from the stratosphere [*Marcy et al.*, 2007].

[23] The HNO_3-O_3 correlation for the in situ data in the tropics is shown in Figure 8. The data are separated into three groups representing air in the lower stratosphere, TTL, and troposphere. The upper and lower boundaries of the TTL, defined using criteria by *Marcy et al.* [2007], are approximately 17.5 km and 14.5 km, respectively. The data in the tropical lower stratosphere (red symbols in Figure 8) reveal a compact linear correlation between HNO_3 and O_3, as described above. The TTL data (blue symbols), which contain the minimum HNO_3 values illustrated in Figure 7, are clustered at the lower end of the stratospheric correlation. The remaining data in the troposphere (green symbols), at altitudes less than 14.5 km, are more variable than the data in the TTL and show no apparent correlation between HNO_3 and O_3. A pronounced feature is the high HNO_3 mixing ratios (>0.05 ppb) at low values of O_3 (<100 ppb). These data are most likely influenced by HNO_3 produced by lightning.

4. Summary

[24] An extensive data set of HNO_3 and O_3 measurements has been collected in the lower and middle stratosphere with in situ instruments onboard the NASA WB-57F and a suite of remote sounding instruments that includes the MkIV, MLS and ACE-FTS. The measurements reveal a compact linear correlation between HNO_3 and O_3 in the midlatitude lower stratosphere. This correlation is robust and comparable between data sets measured using a variety of in situ and remote techniques. Validating remote measurements of HNO_3 by comparing HNO_3-O_3 correlations allows a meaningful comparison between data sets with greatly different sampling volumes. In addition, the use of tracer correlations for validation relaxes the coincidence criteria necessary

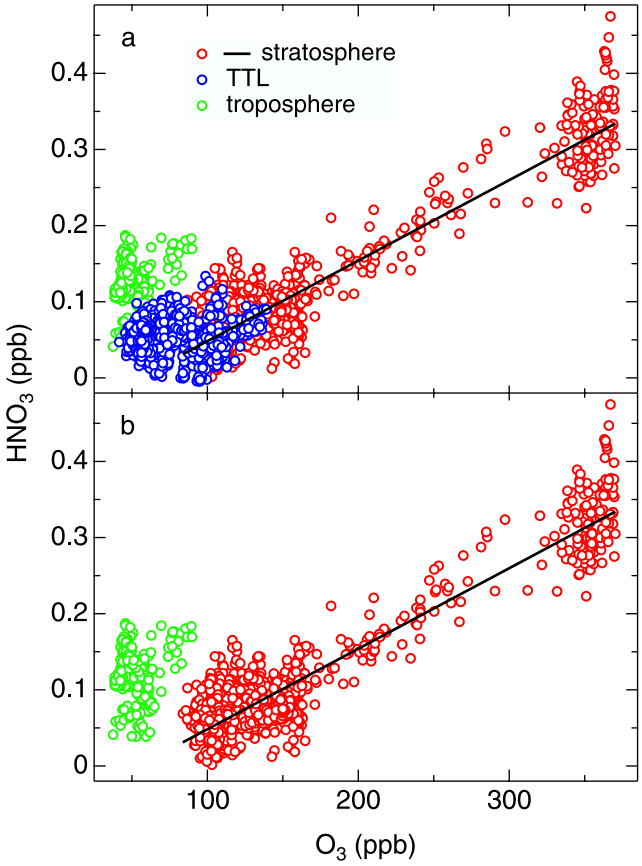

Figure 8. (a) HNO_3-O_3 correlation observed in the tropics. Data points are 10-s averages of in situ measurements onboard the NASA WB-57F. Data in the stratosphere, TTL, and troposphere were selected using criteria described by *Marcy et al.* [2007]. The equation for the linear fit, represented by the black line, is given by $HNO_3 = (0.00106 \pm 1.09 \cdot 10^{-5}) \cdot (O_3) - (0.0575 \pm 0.0018)$ for stratospheric air with ozone mixing ratios less than 370 ppb. (b) Same as Figure 8a, with the TTL data removed to illustrate the separation between the stratospheric and tropospheric data.

when making direct comparisons, allowing meaningful comparisons between data sets that are not closely matched in time and space. As demonstrated here, the use of HNO_3-O_3 correlations increases the value of small data sets in validation or intercomparison studies, and reduces the influence of geophysical variability in those studies. We have shown by example how a well-characterized HNO_3-O_3 correlation can be used to calculate proxy profiles of HNO_3, designated HNO_3*, from in situ ozonesonde profiles. This method offers the advantage that daily variations in the vertical structure of the stratosphere, particularly near the tropopause, will be evident in the ozonesonde data and thus accounted for in the calculation of HNO_3*.

[25] The near-global coverage of satellite-based instruments allows us to assess the latitudinal variation in the HNO_3-O_3 correlation. ACE-FTS and MLS measurements at a range of latitudes in the Northern Hemisphere indicate a strong latitudinal dependence in the correlation resulting from the steady increase in the HNO_3/O_3 ratio as air moves poleward after entering the stratosphere in the tropics. The correlation between HNO_3 and O_3 can also serve as a useful diagnostic for enhanced values of HNO_3 in the upper troposphere. Enhanced HNO_3 mixing ratios as large as 1.5 ppb were observed in the midlatitude upper troposphere that likely result from the oxidation of lightning-produced NO_x. Finally, in situ measurements of HNO_3 in the TTL revealed low mixing ratios (<125 ppt) and a minimum in HNO_3 at altitudes of 14–17 km. This minimum in HNO_3, which has also been observed in remote measurements by the ACE-FTS instrument, has previously been attributed to the convective outflow of air that has been depleted of HNO_3 in the updraft column.

[26] **Acknowledgments.** The authors wish to thank the air and ground crews of the NASA WB-57F aircraft. This work was partially supported by the NASA Upper Atmospheric Research Program and NOAA Atmospheric Chemistry and Climate Program. Work performed at the Jet Propulsion Laboratory, California Institute of Technology, was done under contract with NASA. The Atmospheric Chemistry Experiment (ACE), also known as SCISAT-1, is a Canadian-led mission mainly supported by the Canadian Space Agency and the Natural Sciences and Engineering Research Council of Canada.

References

Bernath, P. F., et al. (2005), Atmospheric Chemistry Experiment (ACE): Mission overview, *Geophys. Res. Lett.*, *32*, L15S01, doi:10.1029/2005GL022386.

Boone, C. D., et al. (2005), Retrievals for the atmospheric chemistry experiment Fourier-transform spectrometer, *Appl. Opt.*, *44*(33), 7218–7231, doi:10.1364/AO.44.007218.

Brasseur, G., and S. Solomon (2005), *Aeronomy of the Middle Atmosphere*, 646 pp., Springer, Dordrecht, Netherlands.

Bregman, A., et al. (1995), Aircraft measurements of O_3, HNO_3 and N_2O in the winter Arctic lower stratosphere during the Stratosphere-Troposphere Experiment by Aircraft Measurements (STREAM) 1, *J. Geophys. Res.*, *100*(D6), 11,245–11,260, doi:10.1029/95JD00219.

Bregman, A., J. Lelieveld, M. M. P. van den Broek, P. C. Siegmund, H. Fischer, and O. Bujok (2000), N_2O and O_3 relationship in the lowermost stratosphere: A diagnostic for mixing processes as represented by a three-dimensional chemistry-transport model, *J. Geophys. Res.*, *105*(D13), 17,279–17,290, doi:10.1029/2000JD900035.

Brewer, A. W. (1949), Evidence for a world circulation provided by the measurement of helium and water vapor distribution in the stratosphere, *Q. J. R. Meteorol. Soc.*, *75*, 351–363, doi:10.1002/qj.49707532603.

Considine, D. B., M. Natarajan, T. D. Fairlie, G. S. Lingenfelser, R. B. Pierce, L. Froidevaux, and A. Lambert (2008), Noncoincident validation of Aura MLS observations using the Langley Research Center Lagrangian chemistry and transport model, *J. Geophys. Res.*, *113*, D16S33, doi:10.1029/2007JD008770.

Dupuy, E., et al. (2008), Validation of ozone measurements from the Atmospheric Chemistry Experiment (ACE), *Atmos. Chem. Phys. Discuss.*, *8*, 2513–2656.

Fahey, D. W., et al. (1990), A diagnostic for denitrification in the winter polar stratospheres, *Nature*, *345*, 698–702, doi:10.1038/345698a0.

Fahey, D. W., et al. (1996), In situ observations of NO_y, O_3, and the NO_y/O_3 ratio in the lower stratosphere, *Geophys. Res. Lett.*, *23*(13), 1653–1656, doi:10.1029/96GL01476.

Farman, J. C., R. J. Murgatroyd, A. M. Silnickas, and B. A. Thrush (1985), Ozone photochemistry in the Antarctic stratosphere in summer, *Q. J. R. Meteorol. Soc.*, *111*, 1013–1025, doi:10.1256/smsqj.47005.

Folkins, I., P. Bernath, C. Boone, L. J. Donner, A. Eldering, G. Lesins, R. V. Martin, B.-M. Sinnhuber, and K. Walker (2006), Testing convective parameterizations with tropical measurements of HNO_3, CO, H_2O, and O_3: Implications for the water vapor budget, *J. Geophys. Res.*, *111*, D23304, doi:10.1029/2006JD007325.

Froidevaux, L., et al. (2008), Validation of Aura Microwave Limb Sounder stratospheric ozone measurements, *J. Geophys. Res.*, *113*, D15S20, doi:10.1029/2007JD008771.

Gao, R. S., et al. (2001), Observational evidence for the role of denitrification in Arctic stratospheric ozone loss, *Geophys. Res. Lett.*, *28*(15), 2879–2882, doi:10.1029/2001GL013173.

Giorgi, F., and W. L. Chameides (1986), Rainout lifetimes of highly soluble aerosols and gases as inferred from simulations with a general circulation model, *J. Geophys. Res.*, *91*(D13), 14,367–14,376, doi:10.1029/JD091iD13p14367.

Hegglin, M. I., and T. G. Shepherd (2007), O_3-N_2O correlations from the Atmospheric Chemistry Experiment: Revisiting a diagnostic of transport and chemistry in the stratosphere, *J. Geophys. Res.*, *112*, D19301, doi:10.1029/2006JD008281.

Hegglin, M. I., et al. (2008), Validation of ACE-FTS satellite data in the upper troposphere/lower stratosphere (UTLS) using non-coincident measurements, *Atmos. Chem. Phys.*, *8*, 1483–1499.

Irie, H., et al. (2006), Validation of stratospheric nitric acid profiles observed by Improved Limb Atmospheric Spectrometer (ILAS)–II, *J. Geophys. Res.*, *111*, D11S03, doi:10.1029/2005JD006115.

Jaeglé, L., D. J. Jacob, Y. Wang, A. J. Weinheimer, B. A. Ridley, T. L. Campos, G. W. Sachse, and D. E. Hagen (1998), Sources and chemistry of NO_x in the upper troposphere over the United States, *Geophys. Res. Lett.*, *25*(10), 1705–1708, doi:10.1029/97GL03591.

Khosrawi, F., et al. (2004), Validation of CFC-12 measurements from the Improved Limb Atmospheric Spectrometer (ILAS) with the Version 6.0 retrieval algorithm, *J. Geophys. Res.*, *109*, D06311, doi:10.1029/2003JD004325.

Krämer, M., et al. (2008), A climatological view of HNO_3 partitioning in cirrus clouds, *Q. J. R. Meteorol. Soc.*, *134*, 905–912, doi:10.1002/qj.253.

Lawrence, M. G., and P. J. Crutzen (1998), The impact of cloud particle gravitational settling on soluble trace gas distributions, *Tellus, Ser. B*, *50*, 263–289.

Marcy, T. P., et al. (2004), Quantifying stratospheric ozone in the upper troposphere with in situ measurements of HCl, *Science*, *304*, 261–265, doi:10.1126/science.1093418.

Marcy, T. P., et al. (2005), Using chemical ionization mass spectrometry for detection of HNO_3, HCl and $ClONO_2$ in the atmosphere, *Int. J. Mass Spectrom.*, *243*, 63–70, doi:10.1016/j.ijms.2004.11.012.

Marcy, T. P., et al. (2007), Measurements of trace gases in the tropical tropopause layer, *Atmos. Environ.*, *243*, 7253–7261, doi:10.1016/j.atmosenv.2007.05.032.

Mari, C., D. J. Jacob, and P. Bechtold (2000), Transport and scavenging of soluble gases in a deep convective cloud, *J. Geophys. Res.*, *105*(D17), 22,255–22,267, doi:10.1029/2000JD900211.

Martin, R. V., et al. (2007), Space-based constraints on the production of nitric oxide by lightning, *J. Geophys. Res.*, *112*, D09309, doi:10.1029/2006JD007831.

Murphy, D. M., et al. (1993), Reactive nitrogen and its correlation with ozone in the lower stratosphere and upper troposphere, *J. Geophys. Res.*, *98*(D5), 8751–8773, doi:10.1029/92JD00681.

Neuman, J. A., et al. (2000), A fast-response chemical-ionization mass spectrometer for in situ measurements of HNO_3 in the upper troposphere and lower stratosphere, *Rev. Sci. Instrum.*, *71*, 3886–3894, doi:10.1063/1.1289679.

Neuman, J. A., et al. (2001), In situ measurements of HNO_3, NO_y, NO and O_3 in the lower stratosphere and upper troposphere, *Atmos. Environ.*, *35*, 5789–5797, doi:10.1016/S1352-2310(01)00354-5.

Newchurch, M. J., M. A. Ayoub, S. Oltmans, B. Johnson, and F. J. Schmidlin (2003), Vertical distribution of ozone at four sites in the United States, *J. Geophys. Res.*, *108*(D1), 4031, doi:10.1029/2002JD002059.

Nightingale, R. W., et al. (1996), Global CF2Cl2 measurements by UARS cryogenic limb array etalon spectrometer: Validation by correlative data and a model, *J. Geophys. Res.*, *101*(D6), 9711–9736.

Popp, P. J., et al. (2004), Nitric acid uptake on subtropical cirrus cloud particles, *J. Geophys. Res.*, *109*, D06302, doi:10.1029/2003JD004255.

Popp, P. J., et al. (2007), Condensed-phase nitric acid in a tropical subvisible cirrus cloud, *Geophys. Res. Lett.*, *34*, L24812, doi:10.1029/2007GL031832.

Proffitt, M. H., et al. (1983), Fast-response dual-beam UV-absorption ozone photometer suitable for use on stratospheric balloons, *Rev. Sci. Instrum.*, *54*, 1719–1728, doi:10.1063/1.1137316.

Ridley, B. A., J. E. Dye, J. G. Walega, J. Zheng, F. E. Grahek, and W. Rison (1996), On the production of active nitrogen by thunderstorms over New Mexico, *J. Geophys. Res.*, *101*(D15), 20,985–21,005, doi:10.1029/96JD01706.

Santee, M. L., G. L. Manney, N. J. Livesey, and J. W. Waters (2000), UARS Microwave Limb Sounder observations of denitrification and ozone loss in the 2000 Arctic late winter, *Geophys. Res. Lett.*, *27*(19), 3213–3216, doi:10.1029/2000GL011738.

Santee, M. L., et al. (2007), Validation of the Aura Microwave Limb Sounder HNO_3 measurements, *J. Geophys. Res.*, *112*, D24S40, doi:10.1029/2007JD008721.

Schneider, J., et al. (1999), The temporal evolution of the ratio HNO_3/NO *y* in the Arctic lower stratosphere from January to March 1997, *Geophys. Res. Lett.*, *26*(8), 1125–1128, doi:10.1029/1999GL900184.

Solomon, S. (1999), Stratospheric ozone depletion: A review of concepts and history, *Rev. Geophys.*, *37*(3), 275–316, doi:10.1029/1999RG900008.

Toon, G. C. (1991), The JPL MkIV interferometer, *Opt. Photonic News*, *2*, 19–21.

Walker, K. A., C. E. Randall, C. R. Trepte, C. D. Boone, and P. F. Bernath (2005), Initial validation comparisons for the Atmospheric Chemistry Experiment (ACE-FTS), *Geophys. Res. Lett.*, *32*, L16S04, doi:10.1029/2005GL022388.

Waters, J. W., et al. (2006), The Earth Observing System Microwave Limb Sounder (EOS MLS) on the Aura satellite, *IEEE Trans. Geosci. Remote Sens.*, *44*, 1075–1092, doi:10.1109/TGRS.2006.873771.

Wolff, M. A., et al. (2008), Validation of HNO_3, $ClONO_2$, and N_2O_5 from the Atmospheric Chemistry Experiment Fourier Transform Spectrometer (ACE-FTS), *Atmos. Chem. Phys.*, *8*, 3529–3562.

P. F. Bernath, Department of Chemistry, University of York, York YO10 5DD, UK.

C. D. Boone, Department of Chemistry, University of Waterloo, Waterloo, ON N2L 3G1, Canada.

D. W. Fahey, R. S. Gao, and L. A. Watts, Chemical Sciences Division, Earth System Research Laboratory, National Oceanic and Atmospheric Administration, 325 Broadway, R/AL6, Boulder, CO 80305, USA.

L. Froidevaux, N. J. Livesey, M. L. Santee, B. Sen, and G. C. Toon, Jet Propulsion Laboratory, California Institute of Technology, Pasadena, CA 91109, USA.

T. P. Marcy, 1962 South Muskego Avenue, Milwaukee, WI 53204, USA.

S. J. Oltmans, Global Monitoring Division, Earth System Research Laboratory, National Oceanic and Atmospheric Administration, Boulder, CO 80305, USA.

P. J. Popp, Leeds School of Business, University of Colorado, Boulder, CO 80309, USA. (peter.popp@colorado.edu)

E. C. Richard, Laboratory for Atmospheric and Space Physics, University of Colorado, Boulder, CO 80303, USA.

K. A. Walker, Department of Physics, University of Toronto, Toronto, ON M5S 1A1, Canada.